P-ISSN 2586-9000
E-ISSN 2586-9027
Homepage : https://tci-thaijo.org/index.php/SciTechAsia
Science & Technology Asia
Vol.28 No.2 April - June 2023
Page: [152-163]
Original research article

The Effect of Building Arrangement Pattern on the Behavior of Air Flow Under Inverse Temperature Condition

Chayanon Serttikul[1], Phadungsak Rattanadecho[2], Tatchanok Prapasawat[3,*]

[1]*Department of Mechanical and Aerospace Engineering, Faculty of Engineering, King Mongkut's University of Technology North Bangkok, Bangkok 10800, Thailand.*
[2]*Department of Mechanical Engineering, Faculty of Engineering, Thammasat University, Pathum Thani 12120, Thailand*
[3]*Center of Excellence in Electromagnetic Energy Utilization in Engineering, Department of Process Chemical and Environmental Engineering, Faculty of Engineering, Pathumwan Institute of Technology, Bangkok 10330, Thailand*

Received 6 April 2022; Received in revised form 19 December 2022
Accepted 16 January 2023; Available online 14 June 2023

ABSTRACT

This research presents the numerical evaluation of heat and mass transfer under the temperature inversion. The study exhibited the moving behaviors of the heat ceiling due to the inverse temperature phenomenon that obstructed the floating of heat and particulate matter from ground level. Moreover, the effect of the building arrangement on the particle matter was also considered. The motion of the thermal layers as a moving boundary problem was considered in conjunction with the energy equation, continuity equation, momentum equation and transport of diluted equations. The results will help in optimizing the design of a city or building arrangement and mitigating the effects of dust accumulation under such conditions. Validation revealed that the velocity field under the inverse temperature conditions from the literature case were consistent with the numerical model by COMSOLTM Multiphysics.

Keywords: Boundary layer; Climates; Moving boundary; Particle diffusion; Temperature inversion

1. Introduction

At the present, the problem of particulate matter has become an important social problem and has affected people's health, especially in cities constructed from many large buildings. The landscape of the city and the pollution from the transportation cause particle accumulation. Moreover, one of the keys which is difficult to control is the problem of temperature inversion. The temperature inversion results from a decreased ability to release heat from the

***Corresponding author:** p.tatchsnok@gmail.com

land at night due to stagnancy of air flow. Normally, it often occurs in late winter. Therefore, the natural heat-transfer decreases significantly which results in a temperature inversion at the morning. Similarly, a heat ceiling obstructs the particles flow from ground level as well. Such a heat ceiling is formed by the presence of a warm air layer in the middle between the cooler air below and above which causes the abnormal temperature hierarchy.

For a few decades, the researches about temperature inversion have been stated as follows. Subrata Kumar Das et al. [1] examined the temperature inversion characterization from radiosonde measurements on the west coast of the Ghats region which has a complex topography. It was found that the temperature inversion can occur in all seasons, but this phenomenon was often found from December to February. K. Frans G. [2] studied the effect of temperature inversion on particle distributions during the winter in Gothenburg, Sweden. The temperature inversions at ground level frequently developed between evening and dawn. They found that the accumulation of the particulate matter peaked during the morning rush hour. However, with such terrain, the dust concentration remained at a high level throughout the day, although it tended to decrease in the late afternoon. H. Koshigoe et al. [3] presented a numerical methodology by using the finite difference method to predict the distribution of temperature in a two-dimensional plane. The study was inspired by the frequent occurrences in Tokyo due to the improper time for cooling of the ground. Julie Malingowski et al. [4] studied the inverse behavior of temperature by considering heat radiation from ground during nighttime and solar heat radiation during daytime in snow regions. SM Bourne et al. [5] analyzed the inverse of temperature at ground level in the Alaska region by using radio observations and found that since 1957, the trend of the occurrence of this phenomenon decreased until the 1980s and increased continuously after that. One of the reasons may be due to the growth of industry and transport. Julie Wallace and Pavlos Kanaroglou [6] examined the effect of temperature inversion on the accumulation of NO2 and particulate matter at ground-level in Hamilton, Canada during 2003-2007. The vertical temperature profiles were collected by using an Atmospheric Infrared Sounder (AIRS). The results showed the accumulation of NO2 and PM 2.5 which increased by 49% and 54% during the night, while PM 2.5 decreased by 4% during the day. However, the accumulation of pollution was significantly less in summer. Wanning Wu et al. [7] studied the temperature profile which induced air pollution in Xianlin District, Nanjing City, China. The data analysis from the aerosol extinction coefficient and AOT (optical density of suspended particles in Atmospheric) cover for temperature, humidity, air pressure, direction of wind and wind speed. The behavior of temperature inversion affects the accumulation of dust at an altitude of not over than 150 meters. If the temperature inversion does not occur, there will be low accumulation of dust and fog. Yunying Li et al. [8] presents the investigation of the temperature inversion in Central of China by using radiosonde data from seven stations during 1990-2010. In the statistical data on the distribution of climate during that time, four-tiered patterns of temperature inversion were found. Namely, there is one temperature inversion layer in the lower troposphere, one in the middle troposphere, and two inversion layers in the upper troposphere. Zengliang Zang et al. [9] studied the accumulation of PM 2.5 at ground-level in Beijing, China by using the aerosol optical depth (AOD) technique. The surface humidity, temperature and atmospheric level were considered to improve the accuracy of the regression model from data collection. Tingting Xu et al. [10] examined the temperature inversion

characteristics in North China on severe pollution days between 2011-2016 by using radiosonde data. They considered the heat transfer and humidity in the atmosphere during the investigation. Xinyuan Feng et al. [11] collected the data of inverse climatic from the ground to an altitude of 5500 meters which affects the local air pollution in Sichuan, China. The geographical location as a river basin adjacent to the Tibetan Plateau, means that the effect of the temperature inversion on the pollution is significant. Lars R. Holeb and Gard Hauge [12] presented a mathematical model to predict the inverse of temperature characteristics at various altitudes with low wind speeds at ground during inversion break up. Sara Janhall et al. [13] measured the particle distribution (size, concentration) of pollutants, including CO, NO, NO_2, and particulate matter in the winter for Nordic urban areas with and without the occurrence of temperature inversion. In the morning, the pollutants tended to decrease when the temperature inversion broke up. Moreover, the inversion layer rises approximately 1 km in height at 2 pm. Purushotham Tukkaraja et al. [14] presented a model for the effects of climate and dust on subsurface mines due to temperature inversion at ground level. The accumulation of dust within the mine, which is below the ground surface, is due to the air flow not rising above the ground level. In addition, there are many case studies for the phenomena of temperature inversion, including [15-18]. Its present dataset between particulate matter accumulation and atmospheric temperature at various altitudes with time. The data is used for statistical analysis to determine the cause of dust accumulation in anticipation of future solutions.

Nevertheless, the study of the effect of the inverse temperature phenomenon by numerical method is limited. Thus, the study of the problem on the basis of Computational Fluid Dynamics (CFD) would reinforce the understanding of problems when the results are explained in conjunction with the knowledge of fluids and heat transfer.

This research presents the numerical investigation of the heat and mass transfer under the inverse temperature conditions. The study shows the behavior of the heat ceiling in the atmosphere due to the inverse temperature phenomenon that interferes with the moving of heat and dust under the different urban planning or building group. The predictions can help in optimizing the design of a city or large building group and help meliorating the effects of dust accumulation under such conditions.

2. Case Studies

Fig. 1 shows the temperature distribution at various altitudes as the temperature inversion phenomenon. It was set as the initial condition before the temperature inversion broke out. In addition, two types of building arrangements in Fig. 2 represent two case studies that affect the behavior of heat and particle movement.

Initially, all domains have an inverse temperature profile according to Fig.1. When time > 0, the gradual decomposition of the inverse temperature profile affects the wider spread of particulate matter.

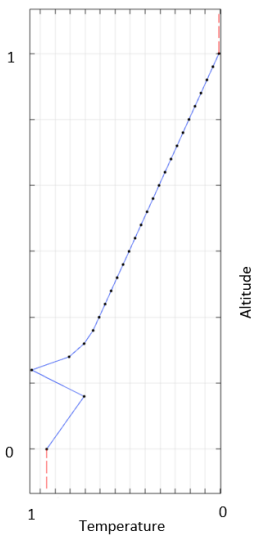

Fig. 1. Dimensionless of temperature gradient (from the temperature between 7 ºC to 31 ºC) at different altitude.

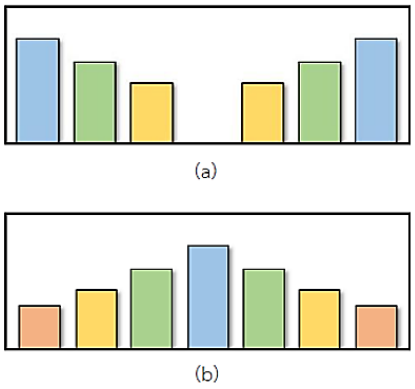

Fig. 2. Two cases study of the building arrangement (a) case study 1 (b) case study 2.

3. Governing Equation, Initial Conditions and Boundary Condition

There are two types of building arrangements in the investigation. The behavior of particle diffusion from the ground into the atmosphere was investigated. The particle diffusion from ground, temperature distribution and convection cell in the atmosphere were compared for the two different building arrangements to see what type of building arrangement is better and can relieve the effects of particle accumulation under the inverse of temperature.

3.1 Governing equation

The governing equations were used to analyze heat and mass transfer, which consist of energy equation, continuity equation, momentum equation and transport of diluted equation respectively, as shown below.

Heat Equation:

$$\frac{\partial T}{\partial t}+\left[u\frac{\partial T}{\partial x}+v\frac{\partial T}{\partial y}\right]=\frac{k}{\rho C_p}\left[\frac{\partial^2 T}{\partial x^2}+\frac{\partial^2 T}{\partial y^2}\right]. \tag{3.1}$$

Continuity Equation:

$$\frac{\partial}{\partial x_i}\left(\rho u_i\right)=0. \tag{3.2}$$

Momentum Equation:

$$\frac{\partial}{\partial x_i}\left(\rho u_i u_j\right)=-\frac{\partial p}{\partial x_i}+\frac{\partial}{\partial x_i}\left(\mu\left(\frac{\partial u_i}{\partial x_i}+\frac{\partial u_i}{\partial x_j}\right)\right)+\frac{\partial}{\partial x_i}\left(-\rho\overline{u_i'u_j'}\right), \tag{3.3}$$

where μ is the coefficient of viscosity and ρ is the density. The Reynolds-averaged momentum equation differs from the general momentum equation in Reynolds-averaged term; that is, the term of Reynolds stresses $\overline{u_i'u_j'}$, this is a term of turbulence flow pattern that occurs under various flow conditions. The Reynolds stress term is a pattern of linear relationship with the rate of change of strain which can be written as an equation based on Boussinesq's hypothesis [20] as follows:

$$-\rho\overline{u_i'u_j'}=\mu_t\left(\frac{\partial u_i}{\partial x_j}+\frac{\partial u_j}{\partial x_i}\right)-\frac{2}{3}\delta_{ij}\left(\rho_k+\mu_t\frac{\partial u_k}{\partial x_k}\right), \tag{3.4}$$

where Eddy viscosity $\left(\mu_t\right)$ is the relationship between the turbulent kinetic energy $\left(k\right)$ and the rate of decline of the turbulent kinetic energy $\left(\varepsilon\right)$. It can be written as follows:

$$\mu_t=\rho c_\mu\frac{k^2}{\varepsilon}, \tag{3.5}$$

k-ε- type fluid turbulence model.

- The equations model for the kinetic energy of turbulence are

$$\frac{\partial}{\partial x_i}\left(\rho k u_i\right)=\frac{\partial}{\partial x_i}\left(\left(\mu+\frac{\mu_t}{\sigma_k}\right)\frac{\partial k}{\partial x_i}\right)+G_k+G_b-\rho\varepsilon. \tag{3.6}$$

- The equations model for the rate of reduction of kinetic energy for turbulence are

$$\frac{\partial}{\partial x_i}\left(\rho\varepsilon u_i\right)=\frac{\partial}{\partial x_i}\left(\left(\mu+\frac{\mu_t}{\sigma_k}\right)\frac{\partial\varepsilon}{\partial x_i}\right)+C_{\varepsilon 1}\frac{\varepsilon}{k}\left(G_k+G_{\varepsilon 3}G_b\right)\frac{\varepsilon}{k}-\rho C_{\varepsilon 2}\frac{\varepsilon}{k}, \tag{3.7}$$

where

$$G_k = -\rho\overline{u_i'u_j'}\left(\frac{\partial u_j}{\partial x_i}\right), \quad (3.8)$$

$$G_b = -g_i \frac{\mu_t}{\rho Pr_t}\cdot\frac{\partial \rho}{\partial x_i}, \quad (3.9)$$

and the various constants within the model are Launder and Sharma's constants [21] as follows:

$$c_\mu = 0.09, C_{\varepsilon 1} = 1.44, C_{\varepsilon 2} = 1.92,$$
$$C_{\varepsilon 3} = 1, \sigma_k = 1, \sigma_\varepsilon = 1.3, \sigma_t = 0.9.$$

Transport of Diluted Equation:

The simulation from the Transport of Diluted Equation shows the behavior of particle diffusion in the air as the concentration parameter. The results are by the initial and boundary conditions as a present.

$$\frac{\partial C}{\partial t} + u\frac{\partial C}{\partial x} + v\frac{\partial C}{\partial y} = D\left[\frac{\partial^2 C}{\partial x^2} + \frac{\partial^2 C}{\partial y^2}\right]. \quad (3.10)$$

The assumptions for the investigation are shown below:

1. The temperature distribution was assumed as two dimensions.
2. The fluid flow was assumed as a turbulent flow and incompressible fluid.
3. The fluid was assumed as the Newtonian fluid.
4. Phase change phenomena are not considered.
5. The phenomena are considered as a transient problem.
6. Boundaries of physical domain were set as no slip condition.

3.2 Initial condition and boundary condition

3.2.1 Buiding arrangement type 1

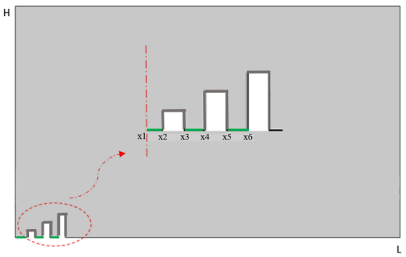

Fig. 3. Physical domain for building arrangement type 1.

Initial Condition (Temperature and Velocity)

$$t = 0,\ u, v = 0\ @0 \le x \le L;\ 0 \le y \le H, \quad (3.11)$$

$$t = 0,\ T = T_i = T(H)\ @0 \le x \le L;\ 0 \le y \le H, \quad (3.12)$$

Initial Condition (Concentration)

$$t = 0,\ C = 0\ @0 \le x \le L;\ 0 \le y \le H, \quad (3.13)$$

Boundary Condition (Temperature and Velocity)

$$t > 0,\ u, v = 0\ @0 \le x \le L;\ y = 0, H, \quad (3.14)$$

$$t > 0,\ u, v = 0\ @x = 0, L;\ 0 \le y \le H, \quad (3.15)$$

$$t \ge 0,\ \frac{\partial T}{\partial y} = 0\ @0 \le x \le L;\ y = H, \quad (3.16)$$

$$t \ge 0,\ \frac{\partial T}{\partial x} = 0\ @x = L;\ 0 \le y \le H, \quad (3.17)$$

$$t>0,\ T=const. \quad \begin{aligned} &@x1\le x\le x2; y=0\\ &@x3\le x\le x4; y=0\\ &@x5\le x\le x6; y=0\\ &@x2\le x\le x3; y=y1\\ &@x4\le x\le x5; y=y2\\ &@x6\le x\le x7; y=y3\\ &@x2;\ 0\le y\le y1\\ &@x3;\ 0\le y\le y1\\ &@x4;\ 0\le y\le y2\\ &@x5;\ 0\le y\le y2\\ &@x6;\ 0\le y\le y3\\ &@x7;\ 0\le y\le y3, \end{aligned} \tag{3.18}$$

$$t>0,\ -q\cdot n=0;\ u\cdot n=0\ @x=0;\ 0\le y\le H. \tag{3.19}$$

Boundary Condition (Concentration)

$$t>0,\ C=C_H\ @X_1\le x\le X_2;\ y=0, \tag{3.20}$$
$$t>0,\ C=C_H\ @X_3\le x\le X_4;\ y=0, \tag{3.21}$$
$$t>0,\ C=C_H\ @X_5\le x\le X_6;\ y=0, \tag{3.22}$$

3.2.2 Building arrangement type 2

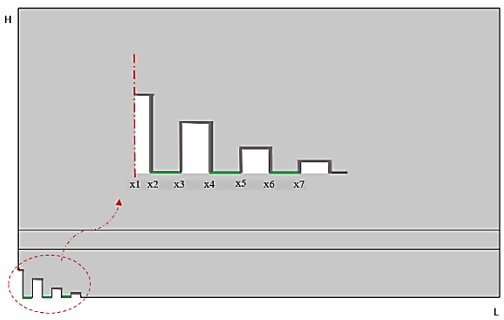

Fig. 4. Physical domain for building arrangement type 2.

Initial Condition (Temperature and Velocity)

$$t=0,\ u,v=0\ @0\le x\le L;\ 0\le y\le H, \tag{3.23}$$

$$t=0,\ T=T_i=T(H)\ @0\le x\le L;\ 0\le y\le H, \tag{3.24}$$

Initial Condition (Concentration)

$$t=0,\ C=0\ @0\le x\le L;\ 0\le y\le H, \tag{3.25}$$

Boundary Condition (Temperature and Velocity)

$$t>0,\ u,v=0\ @0\le x\le L;\ y=0,H, \tag{3.26}$$

$$t>0,\ u,v=0\ @x=0,L;\ 0\le y\le H, \tag{3.27}$$

$$t\ge 0,\ \frac{\partial T}{\partial y}=0\ @0\le x\le L;\ y=H, \tag{3.28}$$

$$t\ge 0,\ \frac{\partial T}{\partial x}=0\ @x=L;\ 0\le y\le H, \tag{3.29}$$

$$t>0,\ T=const. \quad \begin{aligned} &@x2\le x\le x3; y=0\\ &@x4\le x\le x5; y=0\\ &@x6\le x\le x7; y=0\\ &@x1\le x\le x2; y=y1\\ &@x3\le x\le x4; y=y2\\ &@x5\le x\le x6; y=y3\\ &@x7\le x\le x8; y=y4\\ &@x2;\ 0\le y\le y4\\ &@x3;\ 0\le y\le y3\\ &@x4;\ 0\le y\le y3\\ &@x5;\ 0\le y\le y2\\ &@x6;\ 0\le y\le y2,\\ &@x7;\ 0\le y\le y1,\\ &@x8;\ 0\le y\le y1, \end{aligned} \tag{3.30}$$

$$t>0,\ -q\cdot n=0;\ u\cdot n=0\ @x=0;\ 0\le y\le H. \tag{3.31}$$

Boundary Condition (Concentration)

$$t>0,\ C=C_H\ @X_2\le x\le X_3;\ y=0, \tag{3.32}$$
$$t>0,\ C=C_H\ @X_4\le x\le X_5;\ y=0, \tag{3.33}$$
$$t>0,\ C=C_H\ @X_6\le x\le X_7;\ y=0, \tag{3.34}$$

For both case studies, the values of the initial parameter showed as dimensionless are $u,v=0, c_{initial}=10{,}000\frac{mol}{m^3}$, and T according to the relationship shown in Fig. 1, with a variation in the range of 7-31 °C.

4. Numerical Method

The transient problems of the heat and mass transfer under the temperature inversion were solved by the finite element method via the COMSOL™ Multiphysics. The physical domain was considered as two

dimensions with 1 meter of height and 2 meters of width and was discretized by triangular element to approximate the temperature and velocity profile. For acceptable approximation, all governing equations were solved base on enthalpy method and also the mesh was always fixed. The interpolation of the temperature between meshes could be defined as the temperature distribution inside domain. Therefore, the moving boundary layer was defined by the position of the temperature field inversion at any altitudes. Mesh generation was set to be 195,807 elements which the initial time steps were varied during 0.01-1.0 second when the process started to be convergent, and the relative error in the iteration procedures of 10^{-6} was chosen.

The distributions of temperature, velocity and concentration are shown as results in a non-dimensional form as below.

$$x^* = \frac{x}{L}, y^* = \frac{y}{H}, \quad (4.1)$$

$$u^* = \frac{u}{U}, v^* = \frac{v}{V}, \quad (4.2)$$

$$C^* = \frac{c}{C_{max}}, T^* = \frac{T - T_\infty}{T_{max} - T_\infty}, P^* = \frac{P}{\rho V^2}, \quad (4.3)$$

where U and V are velocities at free stream of x and y directions. T_∞ is temperature at free stream. H and L are height and width of domain that were considered to be 500 mm and 3000 mm. For the building group type 1, the ratio of the road distance and the height of the tallest building was 1:3 and the ratio of the road distance and the height of the lowest building was 1:1.

For the building group type 2, the ratio of the road distance and the height of the tallest building was 1:3 and the ratio of the road distance and the height of the lowest building was 1:0.5.

5. Results and Discussion

5.1 Validation

The theory and the simulation results of the mass transport behaviors of the particulate matter under temperature inversion were compared and it was found that the occurrences were consistent.

Fig. 5(a) shows the domain which left and right-hand side are symmetry, the hill act as a trigger and creates the counter current air flow. It was consistent with the simulation which domain is symmetry with the left-hand side of the axis symmetry as Fig. 6(a) and the building group is also acting as a trigger.

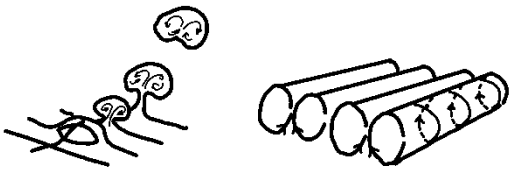

(a) (b)

Fig. 5. Convective Behavior (a) Initiation of a convective flow by a hill, (b) Formation of cloud streets [19].

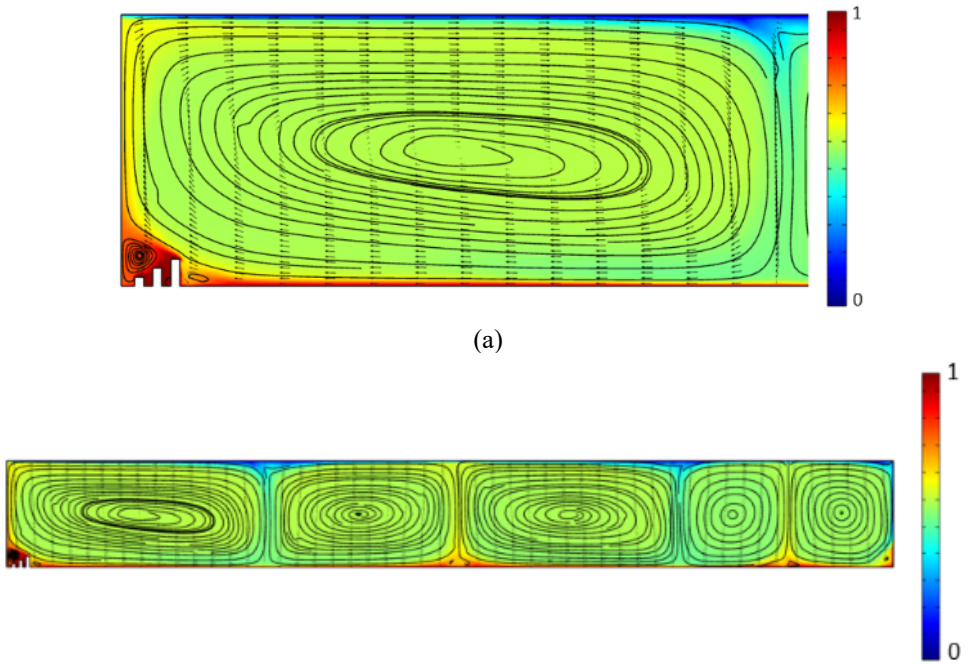

Fig. 6. Convective behavior (a) Initiation of a convective flow by building group, (b) Formation of cloud streets (Right-hand side of building group).

In addition, in the comparison of the theory and the simulation results as shown in Figs. 5(b) and Fig. 6(b), the air vortices that are far away from the hill or the building group display the counter flow characteristic. Moreover, they show that the counter flow increases over a wide area similar to cloud streets. The development of these convection cells occurred since there was little or no horizontal wind, especially in the morning. The convection was less vigorous, and the cells were organized into roll structures aligned parallel to the wind. Therefore, both of the results from Figs. 6(a) and 6(b) are similar and good behavior agreement with the theory from Oke, T.R. [19]. This favorable comparison confirms that the present numerical model is precise.

5.2 Thermal dispersion

The studies of the temperature distribution under the atmospheric inverse temperature were conducted by comparing the behavior between two types of buildings arrangement in urban areas. As consideration at the same time, it was found that the first type of building arrangement showed the temperature field as a thermal dome covering over the building area as in Fig. 7(a). However, the first type was different from the second type of building arrangement as shown in Fig. 7(b). The reason for the heat dome in Fig. 7(a) is that it is the wake region since the building obstructs which causes a large pressure drop, and the low-pressure region inside the building group results in recirculation and backflows with lower Reynolds values than those outside the building block. However, the heat dispersion between the buildings of both types of building arrangement was not quite good. Thus, the distance between buildings is another factor that should be studied in the future.

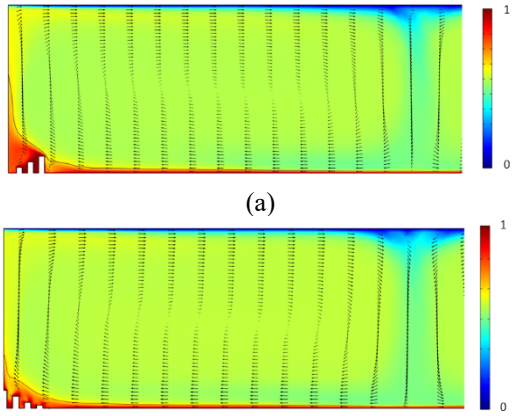

(a)

(b)

Fig. 7. Temperature distribution under inverse of temperature for (a) First type of building arrangement (b) Second type of building arrangement.

As consideration for the second type of building arrangement, the heat ceiling at suburban area or the area which is adjacent to the buildings was lower altitude than the first type since the convection of the ambient was better. It is because the steady air velocity at the same height, especially at low altitudes, outside the second building group was higher than the first type as displayed in Fig. 8.

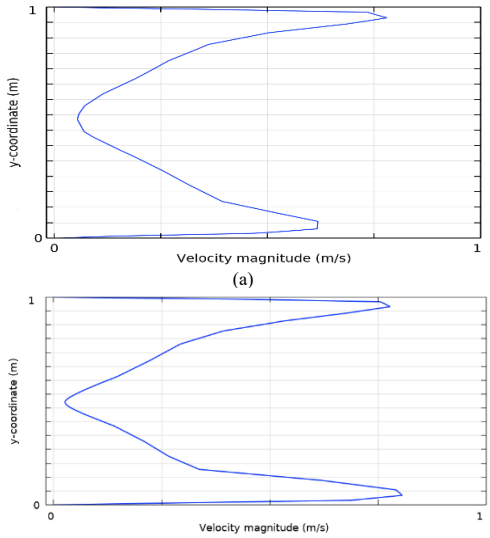

(a)

(b)

Fig. 8. Velocity profile at suburban area for different altitudes with (a) First type of building arrangement (b) Second type of building arrangement.

5.3 Velocity field

In case study 1, the first building arrangement in Fig. 9(a), the smaller counter flow inside the heat dome above the building due to the pressure drop as the building group which blocks the airflow was found. Moreover, there was also a bigger current that was adjacent the building group. These behaviors appeared due to the tallest building of the building group which was a trigger of the air vortex and the temperature distribution as above mentioned.

Therefore, the counter flow moved the particulate matter from the space between the buildings to the air, but most particulate had still circulated inside the heat dome. Whereas the second building arrangement, in Fig. 9(b), significantly affected the dilution of particulate matter in the atmosphere above the building group because the shape of the building arrangement did not obstruct the flow of air in the atmosphere and also resulted in less pressure drop.

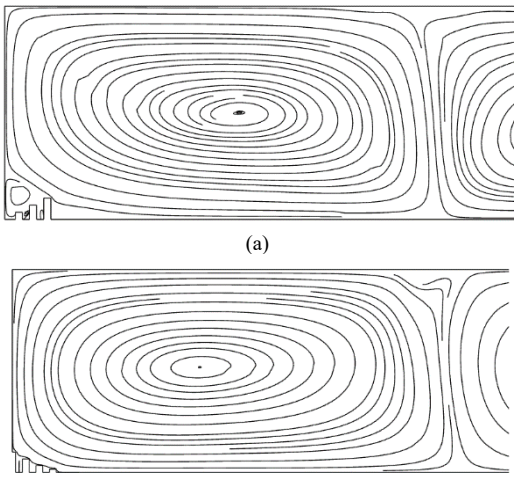

(a)

(b)

Fig. 9. Stream line of air flow for the different of building arrangements (a) First type of building arrangement (b) Second type of building arrangement.

5.4 Concentration

The accumulation of pollutants at the middle of building group type 1 was greater than that of type 2 since the dome shape of the heat ceiling from the wake region at low pressure caused the pollution to move upward into the atmosphere more slowly. In Fig. 10(a), the first building arrangement, the concentrations of the particle at the rural which was far from the building were less diffuse than that compared to Fig. 10(b).

6. Conclusion

The results show that the first building arrangement had less effect on the diffusion of particulate matter out to the suburban plains than that of the second building arrangement. That was because of the heat-ceiling layer above the buildings group.

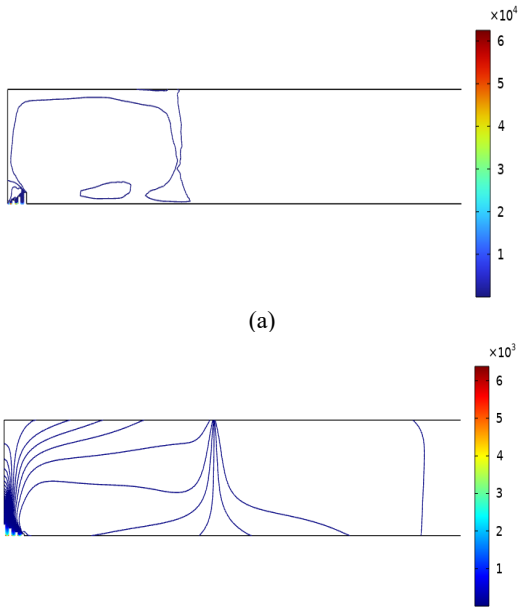

Fig. 10. Concentration diffusion of particulate matter for the different of building arrangements (a) First type of building arrangement (b) Second type of building arrangement.

This is the fact that the velocity of the convection cells inside the heat dome was lower than that outside the building group because of the low pressure in that area (the wake region). In addition, the heat dissipation in the area of the building was also not good. Whereas, if the water spray from top of the building to scrub the particulate matter in the atmosphere could be considered. It is possible that the model of the first building arrangement would control the areas that affected by the pollution more than the other cases.

On the other hand, if the suburban area which is far away from the building also has emissions due to traffic, the first type of building arrangement will have a greater impact on the cumulative amount of pollution at the ground level because the velocity magnitude at the ground level is lower than the case of the second type of building arrangement.

The advantage of this work is to highlight the relationship between the movement behavior of airborne contaminants and the building cluster patterns in order to create inventive ideas for future urban planning. The research studied in the next step is to consider the influence of diffusion of water vapor sprayed from the top of the building group by considering the evaporation of such water vapor, the thermal radiation factors between the ground and the atmosphere.

In addition, the influence of sea winds on the travel distance of airborne contaminants would be considered in the future. The limitation of this research is that the size of the domain that cannot be studied with the actual size of the city. The results were shown as the dimensionless to present the behaviors that occur. However, the trend of behavior is still theoretical and can provide ideas for creative design in the future.

Acknowledgements

This study was supported by Thailand Science Research and Innovation Fundamental Fund.

Nomenclature

x	$x-coordinate$
y	$y-coordinate$
t	$time$
T	$Temperature$
u	$x-coordinate\ velocity$
v	$y-coordinate\ velocity$
k	$Thermal\ conductivity$
ρ	$Fluid\ density$
C_p	$Specific\ heat\ capacity$
P	$Pressure$
μ	$Dynamic\ viscosity$
D	$Diffusion\ coefficient$

References

[1] Subrata KD, Tanaya T, Kizhathur NU, Uriya VM. K, Sanjoy KS. Characteristics of temperature inversion from radiosonde measurements in the Western Ghats region. Atmos Res 2021;250: 105391.

[2] K Frans GO, Patrik UA, Mattias H, Evert L, Lin T, Deliang C, Jan BCP. Urban aerosol evolution and particle formation during wintertime temperature Inversions. Atmos Environ 2009;43: 340-6.

[3] Koshigoe H, Shiraishi T, Ehara M. Distribution algorithm in finite difference method and its application to a 2D simulation of temperature inversion. J Comput Appl Math 2009;232: 102-8.

[4] Julie M, David A, Javier F, Jessica C, Eric S. An observational study of radiation temperature inversions in Fairbanks, Alaska. Polar Sci 2014;8: 24-39.

[5] Stefanie MB, UMA SB, Zhang J, Thoman R. Surface- based temperature inversions in Alaska from a climate perspective. Atmos Res 2010;95: 353-66.

[6] Julie W, Pavlos K. The effect of temperature inversions on ground- level nitrogen dioxide (NO_2) and fine particulate matter (PM2.5) using temperature profiles from the Atmospheric Infrared Sounder (AIRS). Sci Total Environ 2009;407: 5085-95.

[7] Wanning W, Yong Z, Jiahua Z, Jay G, Junliang H. A temperature inversion-induced air pollution process as analyzed from Mie LiDAR data. Sci Total Environ 2014;479-480: 102-8.

[8] Yunying L, Jiping Y, Xingbin S. Tropospheric temperature inversion over central China. Atmos Res 2012;116: 105-15.

[9] Zengliang Z, Weiqi W, Wei Y, Yi L, Fang Y, Chunming W. Estimating ground-level PM2. 5 concentrations in Beijing, China using aerosol optical depth and parameters of the temperature inversion layer. Sci Total Environ 2016;575: 1219-27.

[10] Lutz S. Estimating the effect of air pollution on road safety using atmospheric temperature inversions, J Environ Econ Manag 2019;98: 102250.

[11] Hongwen L, Haitao L, Yu L, Ying L, Zhenhua G. Inversion of distributed temperature measurements to interpret the flow profile for a multistage fractured horizontal well in low- permeability gas reservoir. Appl Math Model 2020;77: 360-77.

[12] Tingting X, Yu S, Mingxu L, Xuhui C, Hongsheng Z, Jianping G, Tong Z. Temperature inversions in severe polluted days derived from radiosonde data in North China from 2011 to 2016. Sci Total Environ 2019;647: 1011-20.

[13] Xinyuan F, Shimin W, Shigong W. Temperature inversions in the atmospheric boundary layer and lower troposphere over the Sichuan Basin, China: Climatology and impacts on air pollution. Sci Total Environ 2020;726:138579.

[14] Purushotham T, Manoj K, Adam F. Simulating temperature inversions in surface mines using computational fluid dynamics. Proc S Dak Acad Sci 2016;95:119-23.

[15] Hiroshi T, Matti S. Surface temperature inversion in the palsa and pounu fields of northern Finland. Polar Sci 2012;6: 237-51.

[16] Madineni VR, Nee JB, Chen WN, Siva KV, Rao PB. Recent observations of mesospheric temperature inversions over a tropical station (13:5◦N; 79:2◦E). J Atmos Sol Terr Phys 2003;65: 323-34.

[17] Jens O, Hanli L, Oleg AG, Dirk O. Mesospheric surf zone and temperature inversion layers in early November 1994. J Atmos Sol Terr Phys 2006;68: 1752-63.

[18] Sultan SAR, Elghribi NM. Temperature inversion in the Arabian gulf and the gulf of Oman. Cont Shelf Res 1995;16: 1521-44.

[19] Timothy RO. Boundary layer climates. 2nd ed. Routledge; 1988.

[20] Boussinesq J, Theory de L'ecoulment tourbillant, memoires presentes par divers Savants Sciences Mathematique at Physiques. Academie de Sci 1877;23: 46-50.

[21] Launder BE., Sharma BI., Application of the energy dissipation model of turbulence to the calculation of flow near spinning disc. Lett Heat Mass Trans 1974;1: 131-8.